ADVANCED FUNCTIONAL MATERIALS
www.afm-journal.de

Organic Thin Film Transistors Based on Highly Dipolar Donor–Acceptor Polymethine Dyes

*Andreas Liess, Lizhen Huang, Alhama Arjona-Esteban, Aifeng Lv, Marcel Gsänger, Vladimir Stepanenko, Matthias Stolte, and Frank Würthner**

Organic thin film transistors (OTFTs) of a series of twenty dipolar donor–acceptor-substituted polymethine dyes (D–A dyes, dipole moments from 3–15 D) are investigated. The employed merocyanine dyes contain a dimethine bridge that is substituted with 1-alkyl-3,3-dimethylindolin-2-ylidene ("Fischer base"), 3-alkyl-2,3-dihydrobenzothiazol-2-ylidene or 1,3-benzodithiole-2-ylidene, respectively, as electron-donating unit and various acceptor heterocycles. These studies show that thin films formed by these D–A dyes upon deposition in high vacuum are all composed of antiparallel π-stacked dimers. However, they are either amorphous, discontinuous or highly crystalline due to the interplay between molecule-substrate and dimer–dimer interactions. With the help of single crystal X-ray analysis, out-of-plane X-ray studies (XRD), selected area electron diffraction (SAED), and atomic force microscopy (AFM), a correlation between the molecular structure, film ordering, and hole charge transport ability can be established. The mobility values are compared to Bässler's disorder charge transport theory and a film growth mechanism is proposed based on DFT calculations and single crystal structures. The results show that with carefully adjusted bulky substituents and high dipolarity an intimate centrosymmetric packing with a slipped, but tight π-stacking arrangement could be realized. This provides two-dimensional percolation pathways for holes and ultimately results in charge carrier mobilities up to 0.18 $cm^2 V^{-1} s^{-1}$.

1. Introduction

Organic semiconductor based electronics have shown rapid development recently which has been driven particularly by the appearance of numerous new organic semiconductor molecules with prominent charge carrier mobility.[1–4] The outstanding prototypes in this field fall in two classes: The first class of materials is based on small molecules which possess extended π-conjugated backbones combined with a dense and well-defined crystalline packing. Prominent examples of this concept are given by π-extended benzothienobenzothiophene compounds for which hole mobilities up to 17 $cm^2 V^{-1} s^{-1}$ in vacuum-processed organic thin film transistor (OTFT) devices could be demonstrated most recently.[5–7] The second class is based on polymers with alternating donor–acceptor (D–A) units which are commonly used to obtain ambipolar devices.[8] Furthermore, this approach is believed to provide strong electrostatic interactions between D and A segments of neighboring molecules that support charge carrier hopping. Indeed, for many D–A copolymers charge carrier mobilities >1 $cm^2 V^{-1} s^{-1}$ have already been achieved, and the highest reported mobilities range at about 10 $cm^2 V^{-1} s^{-1}$.[9–14] These impressive recent improvements in the field open an exciting potential for organic electronics and should stimulate the elucidation of further molecular π-scaffolds that hitherto have been less explored.

It is noteworthy that whilst the D–A concept has been applied to obtain high mobility polymeric semiconductors, small molecules bearing a large dipole moment are still almost absent in the field. According to the disorder charge transport theory, it is implied that molecules with a permanent dipole moment will enlarge the density of states (DOS) distribution and thus decrease the charge carrier mobility.[15] On the other hand lots of dipolar molecules have been investigated in the area of nonlinear optics (NLO) and photorefractive (PR) materials,[16–18] and some showed recently also great promise for organic photovoltaics, first with dye-sensitized solar cells (DSSCs)[19] and more recently also in bulk[20–22] and planar[22,23] heterojunction (BHJ, PHJ) solar cells.

Whilst for NLO and DSSC applications these D–A dyes just act as absorbers, their function is more demanding for BHJ and PHJ solar cells and also to some extent for PR materials because here the D–A dyes have to provide hole transporting domains. In this regard it is puzzling that only very few and little comprehensive studies are available that are dedicated on the charge transport ability and applications of D–A dyes in organic transistor devices.[24,25] Thus, in 1984 Kudo and co-workers reported on vacuum-processed OTFTs for a

A. Liess, Dr. L. Huang, A. Arjona-Esteban, Dr. A. Lv, Dr. M. Gsänger, Dr. V. Stepanenko, Dr. M. Stolte, Prof. F. Würthner
Universität Würzburg
Institut für Organische Chemie
& Center for Nanosystems Chemistry
Am Hubland, 97074, Würzburg, Germany
E-mail: wuerthner@chemie.uni-wuerzburg.de

DOI: 10.1002/adfm.201402678

small series of three merocyanine dyes whose performance was very modest (best device with hole mobility μ = 1.5 × 10^{-5} cm^2 V^{-1} s^{-1}), which was rationalized by the formation of deep traps near the SiO_2-dye interface.[24] Next, in 2012 we were able to demonstrate the first OTFTs with high hole mobility of 0.18 cm^2 V^{-1} s^{-1} in vacuum-processed OTFT devices, however, the study included only one merocyanine dye (**HB255**), in the following named bPr**D3**tBu**A5**.[25] Because this merocyanine dye exhibits a particularly large dipole moment of 13.6 D it can be considered as the perfect antipode to conventional acene, oligothiophene, oligophenylenevinylene, triarylamine, etc. organic semiconductors that are based on unpolar molecules. Accordingly, the impressive results for bPr**D3**tBu**A5** encouraged us to conduct a more systematic study to reveal scope and limitations of such dipolar D–A compounds in organic electronics.

Here we investigate a large series of merocyanine dyes bearing different electron donor and acceptor heterocycles connected to a dimethine bridge (**Scheme 1**). The particular choice of these merocyanines was motivated by our earlier work in organic photovoltaics,[20,22,23] that is, these merocyanine dyes are all strong absorbers, mostly in the region of largest solar flux, and their HOMO and LUMO levels are well-matched to fullerene acceptors for PHJ and BHJ solar cells. Accordingly, we could expect that their HOMO level should also be suitable to provide p-channel transport in OTFTs with gold electrodes at ambient conditions. For these merocyanine dyes we systematically investigated the influence of substituent effects on the merocyanine film ordering and its correlation with the OTFT performance. For our lead structure bPr**D3**tBu**A5** that bears a donor heterocycle based on a derivative of the famous Fischer base (1-alkyl-3,3-dimethylindolin-2-ylidene),[26] a larger variation of alkyl substituents was synthesized to explore the effect of the alkyl chain on the film morphology as well as the corresponding transistor performance.

2. Results

2.1. Materials Synthesis and Molecular Properties

Scheme 1 shows the utilized donor and acceptor groups that are connected by a dimethine bridge to give highly dipolar merocyanine dyes. These dyes could be synthesized in a straightforward way according to the depicted retrosynthetic analysis from easily available methylene bases (blue), electrophilic C1 synthons (*N,N′*-diphenylformamidine, *N,N′*-dimethylformamide/acetic anhydride or formic acid ortho esters),[27] and the respective CH-acidic acceptor compounds (Acc) that were with one exception all of heterocyclic nature. In total, twenty merocyanine dyes bearing different donor and acceptor moieties have been synthesized whose structures are shown in **Figure 1**. The synthetic details and the complete compound characterizations by NMR spectroscopy, mass spectrometry, elemental analysis and UV–Vis spectroscopy are given in the experimental section and the Supporting Information.

The molecular properties that are of interest for applications of these dyes in organic electronics and organic photovoltaics are collected in **Table 1**. These properties include the absorption maxima λ_{max} and absorption coefficients ε_{max} that were derived

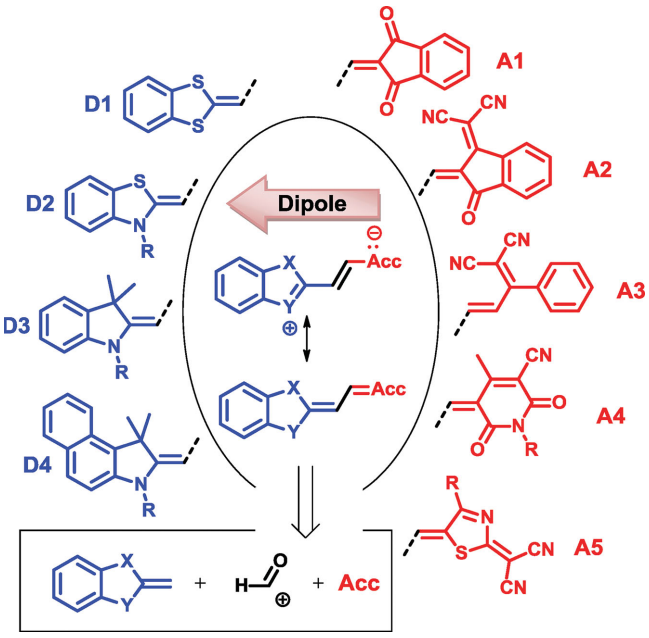

Scheme 1. Dimethine merocyanine dyes based on four different donor (blue) and five different acceptor (red) heterocycles employed in the given study, as well as retrosynthetic analysis (in rectangle) and mesomeric structures (in oval circle).

from UV–Vis spectroscopy and the oxidation and reduction potentials $E_{1/2}$ that were obtained from cyclic voltammetry.

In general all of these D–A dyes show intense absorption bands (ε_{max} > 50000 L mol^{-1} cm^{-1}) in the visible range (**Figure 2** and Supporting Information Figure S1). The comparison of the various acceptors reveals that the 2-(4-alkylthiazol-2(3H)-ylidene)malononitrile acceptor (dyes with acceptor **A5**) leads to the most bathochromically shifted absorption bands (>600 nm), followed by 2-(3-oxo-2,3-dihydro-1H-inden-1-ylidene)malononitrile (dyes **D1A2**, **D3A2**), 1,4-dialkyl-3-cyano-6-hydroxy-2-pyridone (dyes **D1A4**, **D3A4**), 2-benzylidenemalononitrile (dye **D3A3**) and 1,3-indandione (dyes **D1A1**, **D3A1**). Accordingly, there is a quite good correlation between the band gap (inversely correlated to λ_{max}) and the number of methine units between the nitrogen or sulfur donor atoms and the carbonyl or cyano acceptor groups which range from four (**D1A1**, **D3A1**) to eight (dyes with acceptor **A5**). In contrast to these pronounced effects by the acceptor units, the influence of the donor methylene base on the absorption properties is more subtle. In general the λ_{max}-values show smaller variations, for example, 631 nm, 625 nm and 609 nm for **D2A5**, **D3A5**, and **D1A5**, resp., whilst the band shapes are different (Figure 2), leading to pronounced variations in the ε_{max}-values which accordingly do not reflect the tinctorial strength of the dyes but the broadness of the absorption band. These changes in band shape can be related to the electron-donor strength of the resp. methylene bases and the concomitant polarization of the π-scaffold from more polyene-like dyes (broad bands with lower ε_{max}) to more cyanine-like (sharp band with higher ε_{max}) which will be discussed later (EOAM studies).

With cyclic voltammetry at least one oxidative and one reductive wave could be determined for all D–A dyes of this study,

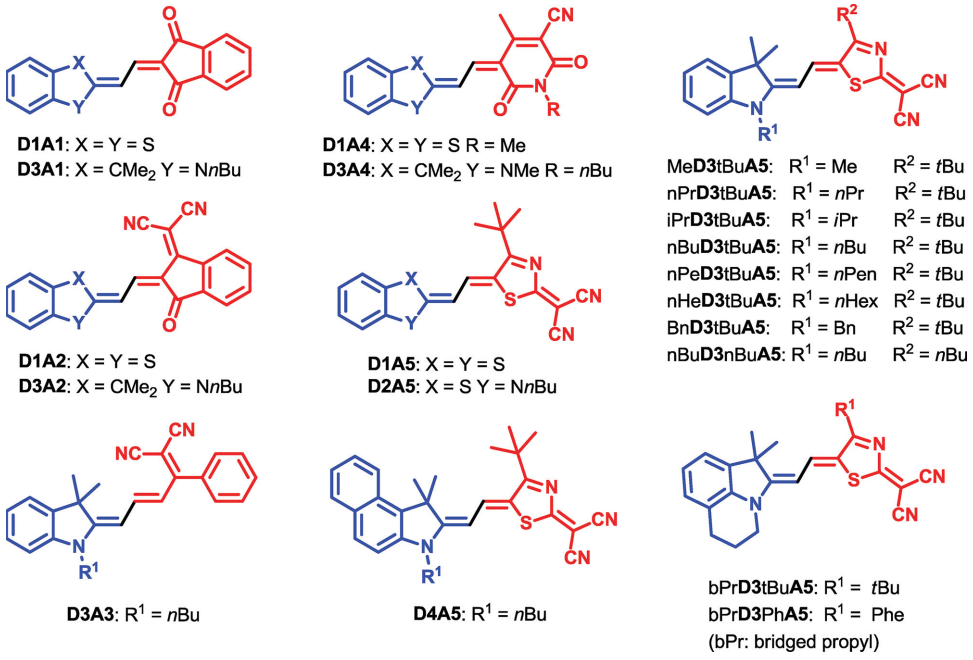

Figure 1. Chemical structures of merocyanine dyes investigated in this study.

albeit the respective redox processes were not always reversible. A comparison between the optical gap (determined from the absorption maxima, i.e., hc_0/λ_{max}) and the electrical gap (determined from the oxidation and reduction potentials, i.e., $E_{1/2,ox}-E_{1/2,red}$) yielded a deviation of about 0.1–0.2 eV, corroborating that the $S_0 \rightarrow S_1$ transition is governed by an electronic excitation from the HOMO to the LUMO level. If we consider that the ferrocene/ferrocenium reference applied in our cyclic voltammetry experiments is located at –5.15 eV vs vacuum level,[31] all investigated D–A dyes are expected to act as electron donors in combination with fullerene acceptors in solar cells or as hole conductors in combination with gold electrodes in OTFTs. Because the electron donor properties are related to the HOMO frontier orbital it is noteworthy that the HOMO level is

Table 1. (Electro-)optical and electrochemical properties of merocyanine dyes[a] determined by UV–Vis[b] and electro-optical absorption[c] spectroscopy as well as cyclic voltammetry[d].

	λ_{max} [nm][b]	ε_{max} [L mol^{-1} cm^{-1}][b]	μ_g [D][c]	$\Delta\mu$ [D][c]	c^2 [1]	$E_{1/2,ox}$ [V][d]	$E_{1/2,red}$ [V][d]
D1A1	517	62 200	2.8	9.2	0.27	0.79[e]	–1.51
D3A1	496[28]	114 600[28]	3.8[28]	3.8	0.40	0.61[e],[28]	–1.94[28]
D1A2	595	61 900	3.9	8.9	0.26	0.84[e]	–1.19[e]
D3A2	576[20b]	66 400[20b]	6.2	4.2	0.40	0.65[20b]	–1.52[20b]
D3A3	533	99 700	9.4	7.9	0.32	0.42[e]	–1.76
D1A4	572	67 400	10.0	8.2	0.30	0.82[e]	–1.23[e]
D3A4	520[17b]	118 000[17b]	12.8[17b]	1.9[17b]	0.45[29]	0.68	–1.71[e]
D1A5	609 663[f]	57 000/34 100[f]	11.7	10.3	0.27	0.58	–1.08[e]
D2A5	631	120 000	15.0	–0.3	0.51	0.39[e]	–1.45[e]
nBu**D3**tBu**A5**	624[28]	128 500	13.3[28]	1.8	0.46	0.43[28]	–1.42[28]
Bn**D3**tBu**A5**	625	112 450	12.5	2.7	0.44	0.46	–1.40
bPr**D3**tBu**A5**	627[25]	146 100[25]	13.6[25]	1.2[25]	0.47	0.38[25]	–1.46[25]
D4A5	640	65 600	13.7	1.8	0.44	0.41	–1.41

[a]Due to similar optical as well as electrochemical properties of dyes **D3A5**, the properties of dyes Me**D3**tBu**A5**, nPr**D3**tBu**A5**, iPr**D3**tBu**A5**, nPe**D3**tBu**A5**, nHe**D3**tBu**A5**, nBu**D3**nBu**A5** and bPr**D3**Ph**A5** are listed in Table S1 (Supporting Information); [b]UV–Vis: CH_2Cl_2, ~10^{-5} M, 298 K; [c]EOAM: 1,4-dioxane, ~10^{-6} M, 298 K, corrected to give "gas phase" dipole moments by Onsager cavity field correction;[30][d]CV: CH_2Cl_2, ~10^{-4} M, 298 K, $N^tBu_4PF_6$ as electrolyte and with reference Fc/Fc^+, the redox values of all other dyes are listed in Table S1; [e]Peak potential of irreversible redox process; [f] Values obtained for the long-wave shoulder of the spectrum (see Figure **2**) by fitting the spectrum with Gaussians.

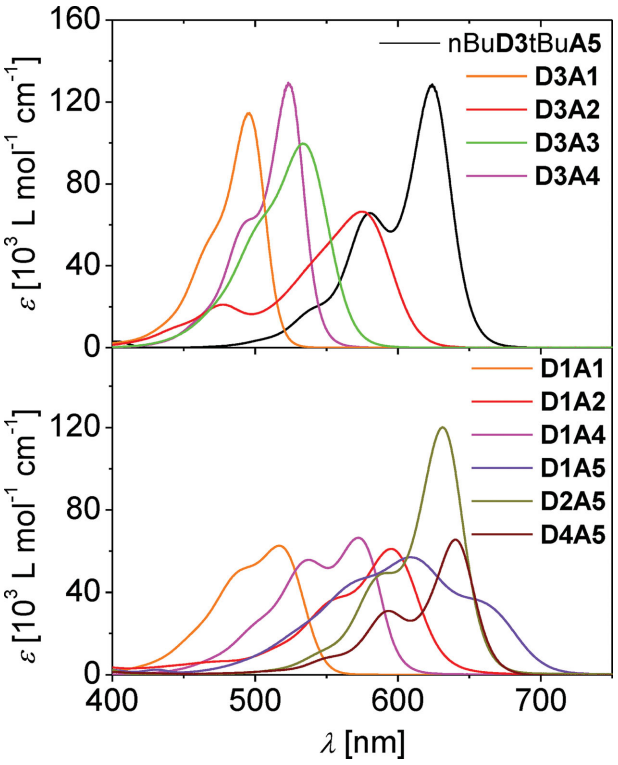

Figure 2. UV–Vis spectra of investigated D–A dyes in CH_2Cl_2 (~10^{-5} M, 298 K). As the dyes of the **D3A5** family show very similar absorption spectra, only the spectrum of nBu**D3**tBu**A5** is included while spectra of all **D3A5** dyes can be found in Figure S1 in the Supporting Information.

located at around −5.6 eV for the majority of the investigated dyes (in particular for almost all members of the extended series of the **A5** acceptor family) and range up to −6.0 eV for 1,3-benzodithiole-2-ylidene dyes **D1A2** and **D1A4**. These results indeed suggest that this methylene base has a lower electron donating power compared to the other two which is surprising due to the wide application of such dithiole donors in tetrathiafulvalenes and related molecules.[32]

For our study the most important molecular property of all dyes given in Table 1 are the ground state dipole moments μ_g that were obtained from electro-optical absorption measurements (EOAM) in 1,4-dioxane and corrected by Onsager cavity field correction to give "gas phase" dipole moments of the respective molecules (Figure S2, Supporting Information).[30] The majority of these dyes have indeed very large dipole moments above 10 D and up to 15.0 D (**D2A5**) which complies with significant transfer of electron density from the donor to the acceptor heterocycles via the conjugated bridge. Only for dyes **D1A1**, **D3A1**, **D1A2**, and **D3A2** the dipole moments remain smaller (2.8–6.2 D) which is explained by the fact that the π-conjugated path reverses its direction in the resp. acceptor units, that is, the carbonyl groups are oriented backwards toward the donor heterocycles. In addition to the ground state dipole moments the EOAM method also provides the change of the dipole moment upon optical excitation of the molecules into the excited singlet state $\Delta\mu$ and—under the assumption that both ground and excited state are composed of complementary contributions of an unpolar and a zwitterionic valence structure (see Scheme 1)—the c^2 value according to Wortmann.[17,33] This value is most convenient to describe the degree of charge transfer from the donor to the acceptor subunit in D–A dyes for merocyanine dyes whose electronic structure is close to the cyanine-limit, that is, $c^2 = 0.5$, where the unpolar and the zwitterionic valence structure (Scheme 1) share equal contributions and all bond lengths are expected to be equal along the polymethine chain.[34] For D–A dyes whose ground state electronic structure is dominated by the unpolar polyene-type structure c^2 values are <0.5 whilst for D–A dyes whose ground state electronic structure is dominated by the zwitterionic structure c^2 values are >0.5. For the given series of D–A dyes we derive c^2 values between 0.26 (**D1A2**) and 0.51 (**D2A5**) by EOAM (Table 1). The fact that the open-chain polymethine dye **D3A3** exhibits a polyene-like electronic structure ($c^2 = 0.32$, i.e., dominating unpolar structure in the ground state and strong bond length alternation) and that the analogous heterocyclic polymethine dye **D3A2** is significantly closer to the cyanine limit ($c^2 = 0.40$) complies with earlier studies that demonstrated how quinoid acceptor heterocycles can be used to polarize D–A dyes towards more zwitterionic structures.[16,17] The fact that polyene-like electronic structures are also shown by the dyes with 1,3-benzodithiole-2-ylidene donor (**D1A1**, **D1A2**, **D1A4**, **D1A5**) reveals a distinct difference between 1,3-benzodithiole-2-ylidene on the one hand and 3-alkyl-2,3-dihydrobenzothiazol-2-ylidene and 1-alkyl-3,3-dimethylindolin-2-ylidene on the other hand. Dyes based on the latter donor units in combination with acceptor heterocycles exhibit always an electronic structure close to or perfectly at the cyanine limit ($c^2 > 0.4$), concomitant with narrow and high intensity (ε_{max}) absorption bands.

2.2. OTFTs on Si/SiO_2 and TPA Modified Substrates

In order to investigate the suitability of all D–A dyes as semiconductors in transistor devices, vacuum processed OTFTs were fabricated in a top-contact bottom-gate configuration (**Figure 3**a). Results on solution-processed OTFTs are not reported here as devices of the twenty merocyanine dyes could rarely be obtained due to solubility problems as well as inhomogeneous film formation on non-functionalized substrates like Si/SiO_2 which, if at all, exhibited only poor performance in the range of 10^{-4}–10^{-7} cm^2 V^{-1} s^{-1}. With the exception of dye **D4A5** which decomposed at the required temperature for sublimation, all other dyes could be deposited by vacuum processing. The details of the fabrication can be found in the experimental section. To optimize the device performance, the dyes were deposited onto heated substrates in the range of 50–120 °C to enable a more crystalline film formation (for the influence of the substrate temperature T_S on the device's performance, see Table S2, Supporting Information). Transfer characteristics were measured at ambient conditions in the saturation regime with a source-drain voltage of $V_{DS} = -50$ V. The effective charge carrier mobilities μ and threshold voltages V_T were determined according to the equation $\mu = (2I_{DS}L/[WC_i(V_{GS}-V_T)^2])$, where W denotes the width, L the length of the transistor channel and C_i the capacitance of the dielectric layer. For every merocyanine, the electrical parameters were averaged over at least five OTFTs and showed a variation less than 10%.

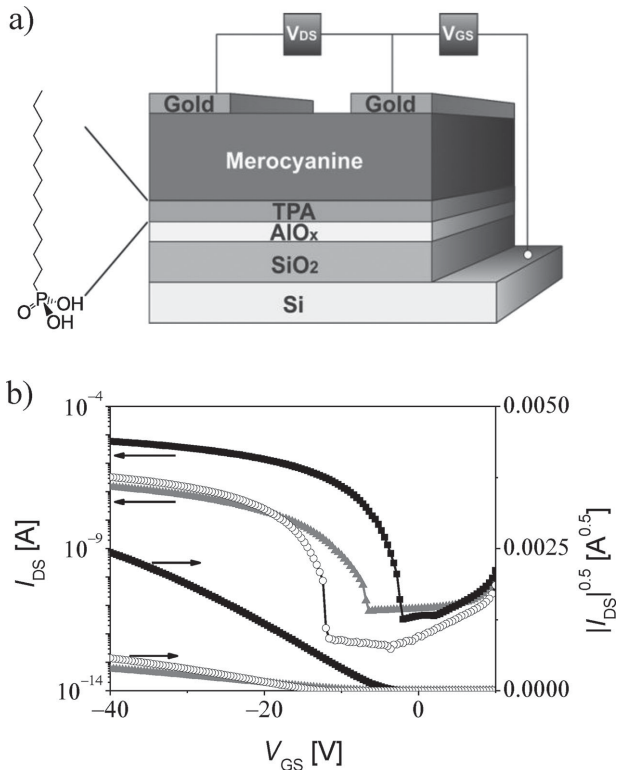

Figure 3. a) Transistor layout in bottom-gate, top-contact configuration and b) transfer curves of the merocyanine **D2A5** (grey triangles), Me**D3**tBu**A5** (open circles) and bPr**D3**tBu**A5** (black squares) based transistors on the TPA modified substrates with V_{DS} = −50 V.

For the working devices, all OTFTs showed hole transport behavior, while the performance varied strongly with the substrate. Table S3 (Supporting Information) shows the determined mobilities, threshold voltages and current on/off ratios (I_{on}/I_{off}) for the devices on Si/SiO_2 substrates. The corresponding transfer curves can also be found in the Supporting Information (Figure S3). Out of the twenty investigated dyes, the devices of five dyes (**D3A1**, **D1A2**, **D3A3**, **D1A4**, nHe**D3**tBu**A5**) showed no field-effect at all. Notably, two of them (**D1A2**, **D1A4**) exhibit the 1,3-benzodithiole-2-ylidene donor which may be taken as an indication that a lack of alkyl side chains prohibits the formation of closed thin films.

The devices of the other fourteen dyes exhibit threshold voltages ranging from −17 up to +1 V, while the hole mobilities and current on/off ratios are in the range of 10^{-4}–10^{-6} cm^2 V^{-1} s^{-1} and 10^2–10^3, respectively. These low mobilities are related to the presence of amorphous thin films according to our AFM studies (vide infra). It appears that there is no clear-cut correlation between the electrical properties of the devices on Si/SiO_2 substrate and the molecular structure of the particular dyes, albeit the lowest value given for 1,3-benzodithiole-2-ylidene dye **D1A1** again supports the idea that the absence of alkyl side chains has a negative effect on the device performance. Accordingly, the only good performing dye **D1A5** of the 3-alkyl-2,3-dihydrobenzothiazol-2-ylidene series (**D1A1**, **D1A2**, **D1A4**, **D1A5**) is the only one that is equipped with a *tert*-butyl group (at the acceptor heterocycle). With regard to the impact of dipolarity on the charge transport properties, it is interesting to see that the hole mobilities slightly increase with increasing dipole moment of the dyes which is indeed at odds with the common hopping transport model of Bässler[15] and will be discussed later.

Whilst the consistently amorphous thin films on Si/SiO_2 substrates showed only small variations of the transistor performance for the whole series of dyes there was a larger differentiation of the electrical properties of the devices on the *n*-tetradecylphosphonic acid (TPA) modified substrates for the various dyes (**Table 2**). On this self-assembled monolayer (SAM) seven dyes (**D3A1**, **D3A2**, **D3A3**, **D1A4**, **D3A4**, **D1A5**, Bn**D3**tBu**A5**) showed no transistor performance at all, two dyes (**D1A1**, **D1A2**) remained on the low level ($\mu \approx 10^{-5}$–10^{-6} cm^2 V^{-1} s^{-1}) as observed on SiO_2, but for the other ten dyes (**D2A5**, Me**D3**tBu**A5**, nPr**D3**tBu**A5**, iPr**D3**tBu**A5**, nBu**D3**tBu**A5**, nPe**D3**tBu**A5**, nHe**D3**tBu**A5**, nBu**D3**nBu**A5**, bPr**D3**tBu**A5**, bPr**D3**Ph**A5**), a significant improvement was observed. The transfer characteristics of the OTFTs of dyes **D2A5**, Me**D3**tBu**A5** and bPr**D3**tBu**A5** are depicted in Figure 3b, the transfer characteristics of all other devices can be found in the Supporting Information (Figure S4). Note, that the transfer characteristics of all OTFTs on the TPA modified substrates showed a mediocre hysteresis of the drain current for the forward and backward measurement cycle (Figure S5, Supporting Information).

Comparing the electrical properties, the values of the hole mobilities and current on/off ratios on the TPA modified substrate are spread over a much wider range as for the devices on Si/SiO_2, peaking at values of μ = 0.18 cm^2 V^{-1} s^{-1} and $I_{on}/I_{off} = 10^6$ for dye bPr**D3**tBu**A5** on the TPA modified substrate.[25] Taking into account the various acceptors of the dyes, it becomes clear, that the best devices were obtained for dyes with the 2-(4-alkylthiazol-2(3H)-ylidene)malononitrile acceptor (**A5** in Scheme 1). All of these dyes belong to the same family of dyes bearing 1-alkyl-3,3-dimethylindolin-2-ylidene (Fischer base) **D3**/**D4** donors (in one case a 3-alkyl-2,3-dihydrobenzothiazol-2-ylidene **D2**) and 2-(4-alkylthiazol-2(3H)-ylidene)malononitrile **A5** acceptors. The consistently good performance observed for the majority of these dyes corroborates their inherent proneness for the formation of crystalline thin films for quite different side chains (e.g., *t*Bu, *n*Bu or Ph at the acceptor heterocycle). Out of the investigated thirteen dyes, the devices of only two dyes (**D1A5**, Bn**D3**tBu**A5**) did not work (again, dye **D4A5** decomposed during the sublimation). The mobilities of the working devices are all larger than 10^{-3} cm^2 V^{-1} s^{-1} and the current on/off ratios are all well above 10^4.

In contrast, OTFTs of dyes with 1,3-indandione **A1** (dyes **D1A1**, **D3A1**), 2-(3-oxo-2,3-dihydro-1H-inden-1-ylidene)malononitrile **A2** (dyes **D1A2**, **D3A2**), 2-benzylidenemalononitrile **A3** (dye **D3A3**) and 1,4-dialkyl-3-cyano-6-hydroxy-2-pyridone **A4** (dyes **D1A4**, **D3A4**) as acceptor moiety either showed no field effect at all or exhibited only low charge carrier mobilities. Out of these seven dyes, the devices of only two dyes (**D1A1**, **D1A2**) showed p-channel behavior, yielding mobilities in the range of 10^{-5}–10^{-6} cm^2 V^{-1} s^{-1} as well as current on/off ratios of the order of 10^2–10^3. These values are comparable to those of their thin films on Si/SiO_2 substrate (see Table S3, Supporting Information).

Comparing the different donors of the dyes bearing the 2-(4-alkylthiazol-2(3H)-ylidene)malononitrile **A5** acceptor, it can be seen that the 1,3-benzodithiole-2-ylidene donor (dye

Table 2. Mobility (μ), threshold voltage (V_T) and current on/off ratio (I_{on}/I_{off}) of the series of merocyanine dye based transistors on TPA modified substrates.[a)]

	T_S [°C]	$T_{Sublimation}$ [°C][b)]	μ [cm^2 V^{-1} s^{-1}][c)]	V_T [V][c)]	I_{on}/I_{off}[c)]
D1A1	65	105	4.3×10^{-5}	0	10^2
D1A2	80	179	3.9×10^{-6}	–3	10^2
D2A5	120	151	0.0043	–11	10^4
Me**D3**tBu**A5**	110	155	0.018	–13	10^5
nPr**D3**tBu**A5**	120	138	0.076	–8	10^6
iPr**D3**tBu**A5**	110	131	0.12	–5	10^6
nBu**D3**tBu**A5**	110	141	0.14	–7	10^5
nPe**D3**tBu**A5**	100	130	0.011	–9	10^5
nHe**D3**tBu**A5**	95	127	0.050	–9	10^6
nBu**D3**nBu**A5**	90	130	0.026	–12	10^5
bPr**D3**tBu**A5**[25]	120	144	0.18	–5	10^6
bPr**D3**Ph**A5**	100	170	0.010	–8	10^5

[a)]Only the parameters of the devices showing a field effect are given in this table. During the sublimation, the deposition rate was gradually increased up to 1 nm min^{-1}, starting with a rate of 0.2 nm min^{-1} at the sublimation temperature $T_{Sublimation}$ for the first 10 nm of the thin film. The substrates were heated to the given substrate temperature T_S; [b)]Sublimation temperature $T_{Sublimation}$ corresponding to a deposition rate of 0.2 nm min^{-1}; [c)]Average value of five transistors. The parameters showed a variation of less than 10%.

D1A5) yields devices with no field effect. For the 3-alkyl-2,3-dihydrobenzothiazol-2-ylidene donor (dye **D2A5**), the mobility of the devices is of the order of 10^{-3} cm^2 V^{-1} s^{-1} and rises above 10^{-2} cm^2 V^{-1} s^{-1} for devices with molecules containing 1-alkyl-3,3-dimethylindolin-2-ylidene (Fischer base) as donor unit (dyes **D3A5**). Concurrently, the current on/off ratio rises one order of magnitude when replacing 3-alkyl-2,3-dihydrobenzothiazol-2-ylidene **D2** by 1-alkyl-3,3-dimethylindolin-2-ylidene (Fischer base) **D3** donors. For the threshold voltage, no such correlation can be obtained. However, there is a loose connection between the values of the threshold voltage and the mobility, as devices with a high mobility tend to have a smaller threshold voltage than devices with a lower mobility.

Taking a closer look on the performance of the series of the best dyes **D3A5**, an influence of the variation of the alkyl chain substituent can be established. For a linear alkyl chain, the mobility rises with increasing chain length from the methyl substituent (Me**D3**tBu**A5**) over *n*-propyl (nPr**D3**tBu**A5**) to *n*-butyl (nBu**D3**tBu**A5**) with a peak mobility of $\mu = 0.14$ cm^2 V^{-1} s^{-1}. Further elongation of the alkyl chain to *n*-pentyl (nPe**D3**tBu**A5**) and *n*-hexyl (nHe**D3**tBu**A5**) results in a decline of the mobility. When substituting the alkyl chain with a benzyl group (Bn**D3**tBu**A5**), the devices exhibit no field effect at all. For the different configurations of the attached propyl group (dyes nPr**D3**tBu**A5**, iPr**D3**tBu**A5** and bPr**D3**tBu**A5**), the devices show an improvement from *n*-propyl (nPr**D3**tBu**A5**) over *i*-propyl (iPr**D3**tBu**A5**) to the bridged propyl (bPr**D3**tBu**A5**) configuration with the obtained peak mobility of $\mu = 0.18$ cm^2 V^{-1} s^{-1} for dye bPr**D3**tBu**A5**.

2.3. Film Morphology and Microstructure

Our previous results indicated that the devices fall into two classes, that is, devices with $\mu > 10^{-3}$ cm^2 V^{-1} s^{-1} can be attributed to crystalline thin films and those devices with $\mu < 10^{-4}$ cm^2 V^{-1} s^{-1} can be attributed to amorphous thin films. In order to obtain confirmation for these conclusions, the molecular films with a nominal thickness of 30 nm were analyzed by atomic force microscopy (AFM) and representative results are shown in **Figure 4**.

Figure 4a,b shows the morphology of thin films of dyes **D3A1** and **D3A2** on Si/SiO$_2$. In the case of dye **D3A1**, no continuous film but rather unconnected domains were formed during the deposition process, hence providing no percolation pathways for charge carriers. This explains quite reasonably, why devices of some dyes did not show any semiconducting behavior. AFM images of smooth thin films with no structural features were obtained for dye **D3A2** on Si/SiO$_2$ which is typical for thin films of the investigated dyes on Si/SiO$_2$ exhibiting poor OTFT performance (Table S3, Supporting Information). The very similar, yet low mobility values (10^{-4}–10^{-6} cm^2 V^{-1} s^{-1}) of OTFT devices on Si/SiO$_2$ suggest that they are mainly governed by the amorphous thin film morphology despite their different molecular properties or packing.

On the TPA modified substrate, the thin films of dyes **D3A1** and **D3A2** (Figure 4c,d) showed a dewetting of the substrate, forming droplet-like grains which again are not interconnected. Therefore, those devices did not show any field effect. However, for the other devices with $\mu > 10^{-3}$ cm^2 V^{-1} s^{-1} the AFM images clearly show a structured surface. Thin films of dyes **D2A5** and Me**D3**tBu**A5** exhibit small features (Figure 4e,f). Small needle-like domains with grain lengths of up to 0.5 µm can be seen for both thin films. Imaging the surface of the thin film of dye Me**D3**tBu**A5** was challenging due to upright standing needles and its resulting high roughness (RMS ≈ 45–85 nm). Both features explain well the fact that mobilities of the corresponding OTFTs were among the lowest values in this series of **D3A5** dyes.

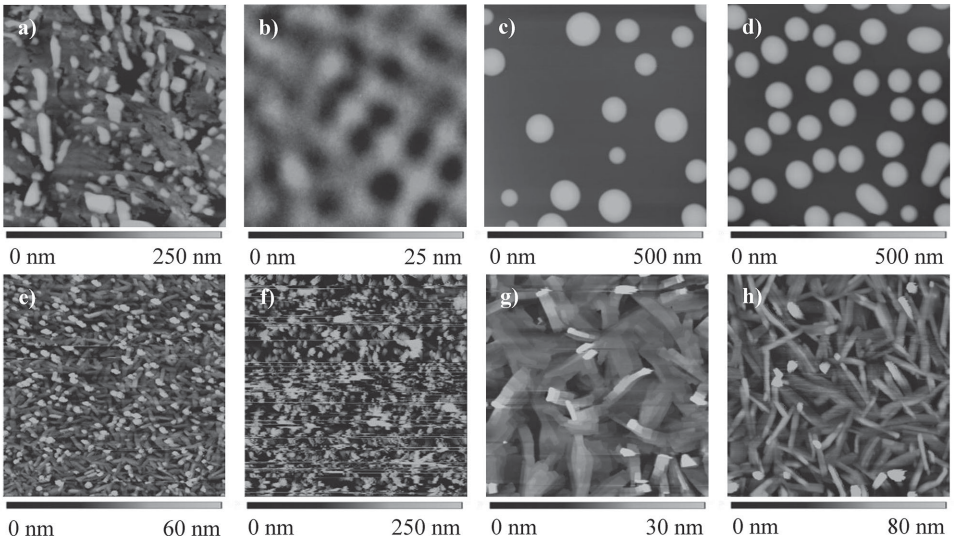

Figure 4. AFM height images of 30 nm vacuum deposited thin films (nominal thickness) of a) **D3A1**, b) **D3A2** on Si/SiO_2, as well as c) **D3A1**, d) **D3A2**, e) **D2A5**, f) Me**D3**tBu**A5**, g) nBu**D3**tBu**A5**, h) bPr**D3**tBu**A5** on the TPA modified substrates. Each image scales to 5 μm × 5 μm.

On the other hand, the thin films of almost all other **D3A5** dyes clearly show larger sized grains and layered structures which explain well the higher charge carrier mobilities of their devices. For dye nBu**D3**tBu**A5** a clear terrace-like morphology with grain sizes up to 2 μm and a step height of 1.1 ± 0.2 nm can be observed (Figure 4g). For dye bPr**D3**tBu**A5**, the morphology of the thin films is similar to that of the film of dye nBu**D3**tBu**A5** although showing slightly smaller rod-like grains and not so well-defined terrace-like structures (Figure 4h). This does not correspond with the fact that the OTFT of dye bPr**D3**tBu**A5** shows a slightly higher mobility as that of dye nBu**D3**tBu**A5** and demonstrates that the film morphology gives good explanations for the different mobility values but is clearly not enough to explain every difference.

For the family of dyes **D3A5**, the influence of the substituent at the donor moiety on the thin film morphology is depicted in Figure S6 (Supporting Information). For an attached methyl group (dye Me**D3**tBu**A5**) the surface of the thin film shows small crystalline regions and is very rough. However, when elongating the alkyl chain, the surfaces become smoother and the grain sizes rise with increasing length of the alkyl chain from methyl (Me**D3**tBu**A5**) to *n*-pentyl (nPe**D3**tBu**A5**). Further elongation of the alkyl chain to *n*-hexyl (nHe**D3**tBu**A5**) leads to frayed islands while a substitution of the alkyl chain with a benzyl group (Bn**D3**tBu**A5**) induces a dewetting of the substrate. Note that for the thin film of dye nPe**D3**tBu**A5** the grain size of the islands are the biggest of all investigated thin films. However, as the inlet in Figure S6f shows, there are cracks in the thin film, surely affecting the percolation pathways.

2.4. Single Crystal X-Ray Analysis

In order to further investigate the diversified device performance, single crystal structures of compounds **D3A1**, **D3A2**, **D3A4**, Me**D3**tBu**A5**, nBu**D3**tBu**A5**, nHe**D3**tBu**A5** and bPr**D3**tBu**A5** were determined. All crystals were grown from solution by either slow evaporation of the respective solvent or slow diffusion of a bad solvent into the solution of the respective dye (for further information, see Supporting Information).

From the X-ray structures of these seven molecules the bond length alternation (BLA)[34] for the three C–C bonds between donor and acceptor heterocycles could be calculated and correlated to the "gas phase" c^2 values determined for the molecules in solution. Here, a BLA $<\Delta r> = 0$ suggests the molecule being in the cyanine limit, that is, $c^2 = 0.5$, whereas a large negative BLA suggests a ground state dominated by the zwitterionic structure. However, no quantification, that is, calculation of c^2 values from BLA values to quantify the offset from the cyanine limit, can be done. The obtained BLA values are given along with the measured bond lengths in Table S4 (Supporting Information) and it can be seen that dyes **D3A1** and **D3A2** exhibit the smallest bond length alternation with a value close to zero of $<\Delta r> = -0.001$ Å and $<\Delta r> = -0.005$ Å, respectively. Dye **D3A4** as well as the four dyes of the **D3A5** family show larger negative BLA values between $<\Delta r> = -0.015$ Å and $<\Delta r> = -0.025$ Å. Comparing the BLA values to the "gas phase" c^2 values (Table 1), one notices that the structure of all dyes in the solid state is shifted towards the more zwitterionic resonance structure (Scheme 1) as indicated by the negative $<\Delta r>$ values. Owing to the more polarizing solid state environment the dyes **D3A1** and **D3A2** with the lowest c^2 values of 0.40 are now the ones closest to the cyanine limit (corresponding to $c^2 = 0.5$) in the crystalline state.

The packing of dyes **D3A1**, **D3A2**, Me**D3**tBu**A5** and nBu**D3**tBu**A5** is depicted in **Figure 5** (the other crystal structures can be found in the Supporting Information, Figure S7) with the acceptor part of the molecule colored red, the donor moiety colored blue and their alkyl chain in grey. Note that due to a slight twisting of some molecules along the polymethine bridge and concomitant lack of overall planarity, the given π–π-distances were calculated for the spacing between parallel acceptor moieties. One common feature which can be found in all of the obtained crystal structures is the antiparallel

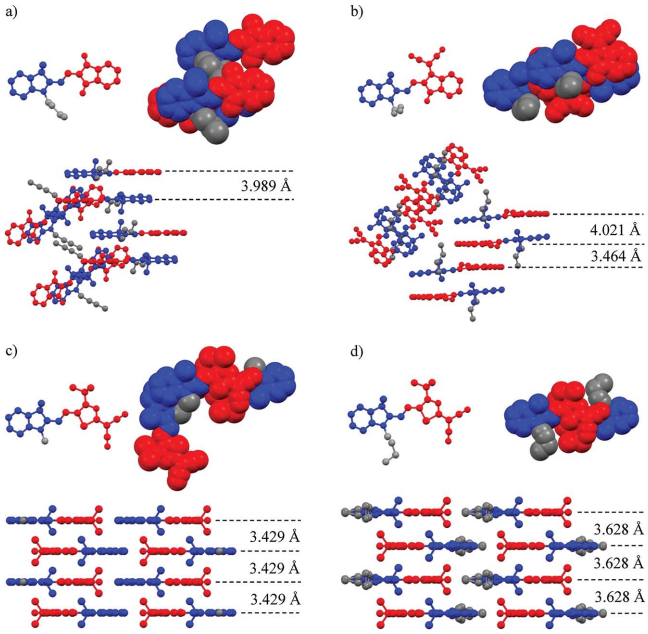

Figure 5. Crystal packing of merocyanine dyes a) **D3A1**, b) **D3A2**, c) Me**D3**tBu**A5** and d) nBu**D3**tBu**A5** with the acceptor part of the molecule colored red, the donor moiety colored blue and the alkyl chain at the donor colored grey. Shown is the molecular structure with packing of the respective closest dimers as well as side views to reveal the corresponding π–π-stacking distances of the molecules to their closest neighbors (calculated for the acceptor moieties).

alignment of neighboring molecules, indicating that the ground state dipole moment has a major impact on the packing of the dyes. Accordingly, as suggested in a previous concept article,[35] this antiparallel dimer motif may be regarded as a "supramolecular synthon"[36] albeit the arrangement of the molecules is not as precisely defined by the dipole moments of molecules as for instance for hydrogen bonds.[36] Thus, at a closer look, two distinct packing motifs can be distinguished: The acceptor moiety of one molecule lies either on top of a donor moiety (Figure 5a,b: **D3A1**, **D3A2**; Figure S7a: **D3A4**) or on top of another acceptor moiety (Figure 5c,d and Figure S7b,c: **D3A5** series) of the closest neighboring molecule. Additionally, the π–π-distances of the two adjacent molecules is either different (Figure 5a,b: **D3A1**, **D3A2**; Figure S7a: **D3A4**) or (almost) equal (Figure 5c,d and Figure S7b,c: **D3A5** series).

The first case—one next neighbor is located at a significantly closer distance and the acceptor lies on top of the neighbor's donor moiety—may be regarded as a situation, where the dipolar interaction energy between two dyes has been optimized at the expense of the other now more distant surrounding molecules. Despite of larger intermolecular distances and a more pronounced slipping of the further neighbor we may still recognize a continuous one-dimensional π-stack of the dimer units for dyes **D3A2** and **D3A4**. In contrast, for dye **D3A1**, the packing motif consists only of an isolated antiparallel stacked dimer unit with a π–π-distance of 3.989 Å, whereas the molecules of this dimer unit have no overlap with the π-surfaces of the other neighboring molecules.

The second case, found for all dyes of the **D3A5** family, shows a brickwork-type packing pattern with four next neighbors located at almost the same π–π-distance. This packing resembles a more balanced allocation of the dipolar interaction energy between all neighboring dyes with π–π-overlap in the crystal, but requires a significant slipping between the molecular centers, which is supported by the bulky *tert*-butyl and $C(Me)_2$ subunits of these molecules. Because of the antiparallel orientation of neighboring D–A molecules this packing motif affords acceptor-acceptor and donor–donor contacts between the π-stacked molecules.

Further analysis of the molecular long-range packing shows that there are again two distinguished arrangements, one showing stacks of dimers which are tilted and twisted against each other (Figure 5a,b: **D3A1**, **D3A2**; Figure S7a: **D3A4**), the other showing a two-dimensional layer-like structure (Figure 5c,d and Figure S7b,c: **D3A5** series).

In this layered packing motif (Figure 5c,d and Figure S7b,c: **D3A5** series), isolated dimers cannot be distinguished as each next neighboring molecule has (almost) the same π–π-distance. These π–π-distances are 3.429 Å for dye Me**D3**tBu**A5** and 3.628 Å for dye nBu**D3**tBu**A5**. In both cases, the molecules have a perfectly planar backbone and the acceptor parts overlap, while for dye Me**D3**tBu**A5** the donor parts overlap additionally. For dye nHe**D3**tBu**A5** the analysis is not that simple, as there are two different conformations of the molecule present in the crystal (see Figure S7b), one showing only a small twist between the donor and the acceptor part of 2.8°, the other showing a larger twist of 8.9°. Furthermore, the π–π-distance is not identical for both conformations and varies slightly. However, the layer-like packing is still present. The analysis of the crystal structure of bPr**D3**tBu**A5** indicates a layered structure as well, although the crystal incorporated the solvent $CHCl_3$ from which the crystal was grown, therefore not showing perfectly aligned planes with a distance of about 3.389–3.397 Å.

It is quite remarkable that all merocyanine dyes with high performance in OTFTs ($\mu > 10^{-3}$ cm^2 V^{-1} s^{-1}) show the second type of 2D packing motif. When comparing these results to the OTFT performances of the devices and the AFM results, it becomes clear that the thin film of those dyes, which show a packing motif with tilted stacks or isolated dimers, also show no field effect on the TPA modified substrate due to a dewetting of the substrate. However, the thin films of **D3A5** dyes with the layered single crystalline structure show all high field effect mobilities of $\mu > 0.01$ cm^2 V^{-1} s^{-1}.

2.5. XRD and SAED Studies

With regard to the issues of molecular packing in the thin films as well as their molecular orientation on the substrate, out-of-plane X-ray diffraction (XRD) and selected area electron diffraction (SAED) measurements were performed and correlated to the single crystal structures. The two techniques can be regarded as complementary as XRD gives information about planes which are oriented parallel to the substrate while SAED shows diffraction for planes which are standing upright on the substrate. Because crystalline films with good transistor performance could only be obtained for dyes of the **D3A5** family, our further studies were focused on members of this class of compounds. Please note that the result of the SAED analysis

given here for dye bPr**D3**tBu**A5** is slightly different to the one given in a previous publication.[25] This is due to a more refined measurement of a sample with only 5 nm thin film to investigate the first few monolayers.

Figure 6 shows the XRD patterns of the thin films of compounds Me**D3**tBu**A5**, nBu**D3**tBu**A5** and bPr**D3**tBu**A5** on TPA modified substrates including the corresponding simulated powder spectra for Me**D3**tBu**A5** and nBu**D3**tBu**A5** which were derived from the single crystal structure using the software Mercury.[37] The XRD pattern of the dye Me**D3**tBu**A5** shows only one clear peak at 7.3° which correlates well with the rough surface and poor crystallinity of the thin film and can be assigned to the (020) peak of the simulated powder spectrum. When analyzing the XRD pattern of the thin film of dye nBu**D3**tBu**A5**, there are three clear diffraction peaks at 8.0°, 16.0°, and 24.1°, corresponding to the crystalline (10–1), (20–2), and (30–3) planes. The number of peaks as well as their intensity and line width indicate a much higher degree of crystallinity in the film than for Me**D3**tBu**A5** which is further supported by the fact that the thin film of dye nBu**D3**tBu**A5** also showed the largest grains in the AFM images. The thin film of dye bPr**D3**tBu**A5** shows two distinct peaks at 9.1° and 9.6°. Such close lying peaks could mean

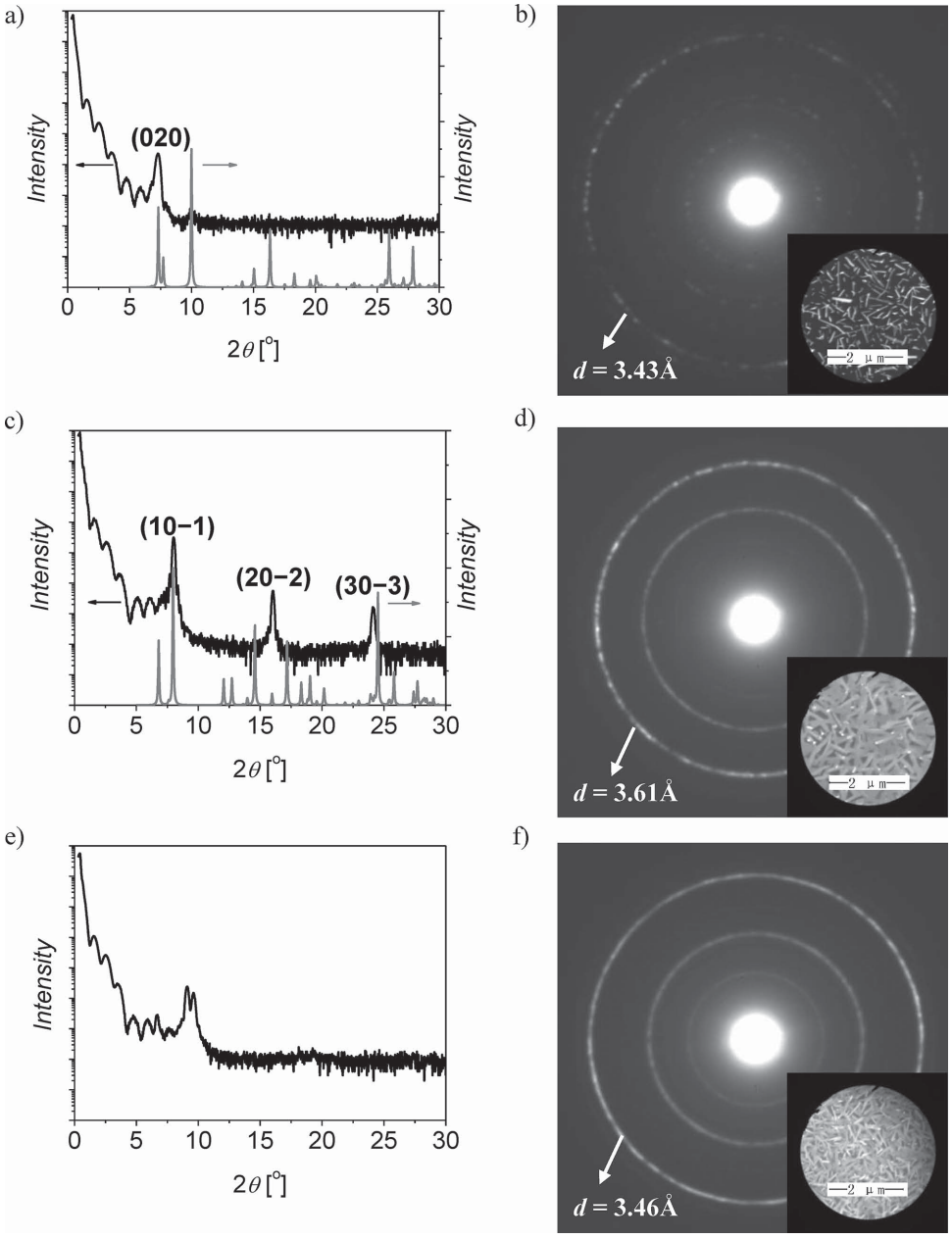

Figure 6. XRD patterns (black lines) for 30 nm thin films on TPA modified substrates with corresponding powder spectra (grey lines) simulated from single crystal structures (a,c,e) as well as corresponding SAED diffraction patterns for 5 nm thin films on TPA modified substrates with calculated interplanar distances *d* (b,d,f) of dyes Me**D3**tBu**A5** (a,b), nBu**D3**tBu**A5** (c,d) and bPr**D3**tBu**A5** (e,f). The inlets in (b,d,f) show the region of the thin films from TEM measurement for which SAED experiments were performed.

that two orientations of crystallites with equal contributions to the thin film phase exist in the thin film. Because we could not grow a solvent-free single crystal for this dye a more in-depth analysis is not possible for this material.

Complementary to the above stated results of the XRD analyses, SAED measurements give insights into the arrangement of planes perpendicular to the surface. Strong diffraction cycles were observed for all three thin films and indicate the polycrystalline nature of these, which is supported by the AFM results (Figure 4) as well as the morphology of the regions which were used for SAED, obtained by transmission electron microscopy (TEM; inlet in Figure 6b,d,f). This is reasonable, as the vacuum deposition is a nondirectional deposition technique. From the distance of the diffraction cycles to the center spot, the corresponding interplanar distances were calculated and showed to be in good agreement with the π–π-distances from the single crystal structures (Figure 5 and Supporting Information Figure S7). In this regard, the diffraction pattern of dye nBu**D3**tBu**A5** indicates a lattice spacing of 3.61 Å whereas compounds Me**D3**tBu**A5** and bPr**D3**tBu**A5** give smaller lattice spacings of 3.43 Å and 3.46 Å, respectively. All three values are in excellent agreement with the π–π-distances found in single crystals which are 3.63 Å for nBu**D3**tBu**A5**, 3.43 Å for Me**D3**tBu**A5**, and 3.40 Å for bPr**D3**tBu**A5**. The shorter π–π-distances for Me**D3**tBu**A5** and bPr**D3**tBu**A5** are reasonable as the long butyl chain of nBu**D3**tBu**A5** possesses more flexibility and gives rise to a larger steric effect compared to the bridged propyl and methyl group. This might also be the reason why the devices of compound bPr**D3**tBu**A5** still could achieve high mobilities although the thin film morphology appears not as good as the one of compound nBu**D3**tBu**A5**.

From the XRD, SAED and single crystal results, the orientation of the molecules Me**D3**tBu**A5** and nBu**D3**tBu**A5** on the TPA modified substrate can be deduced and are depicted in **Figure 7**. The diffraction planes observed in the XRD experiments are hereby oriented almost parallel to the substrate ((020) for dye Me**D3**tBu**A5** and (10–1) for dye nBu**D3**tBu**A5**) whereas the diffraction planes from the SAED measurements, arising from the planes where the π–π-stacking occurs, are almost perpendicular to the substrate. The single crystal results show that the π–π-stacking lies in the direction of the *c*-axis for dye Me**D3**tBu**A5** whereas for dye nBu**D3**tBu**A5** it lies in the direction of the *b*-axis. From these results we conclude that both molecules adopt an edge-on orientation on the TPA modified surface within the crystalline domains of the thin films and show a close π–π-stacking along the direction of the transistor channel which enables efficient charge carrier transport.

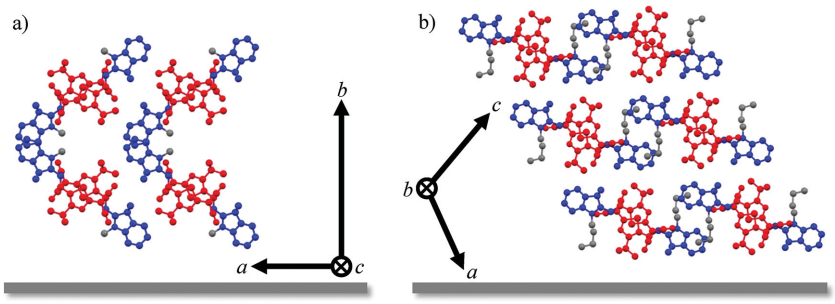

Figure 7. Orientation of the molecules within the thin film of dyes a) Me**D3**tBu**A5** and b) nBu**D3**tBu**A5** on TPA modified substrates based on the XRD, SAED and single crystal results. Additionally given are the respective axes of the single crystal structures.

3. Discussion

3.1. Description of the Disorder Charge Transport Theory

The disorder charge transport theory of Bässler implies that using molecules with a permanent dipole moment in semiconducting layers will result in only moderate charge carrier mobilities due to a broadening of the density of states distribution.[15] The theoretical model describes the movement of the charge carrier as a hopping process between energetic sites (here related to the HOMO levels) and is therefore not limited to any experimental setup or class of materials. With the assumption of non-interacting dipoles and consideration of other parameters (e.g., the average distance of the organic semiconductor molecules in a polymer matrix), the model predicts a scaling of the charge carrier mobility with the dipole moment according to $\log \mu \sim -\mu_g^2$.[15a] Experimental support for this seminal theory was given by data from Sugiuchi and Nishizawa who reported the decrease of charge carrier mobility in molecularly doped polycarbonate (1:1 ratio by weight).[38] In this study, only molecules with small dipole moments (μ_g up to 5.56 D) were investigated and it was assumed that the dipoles were non-interacting due to the spatial displacement of the molecules in the polycarbonate matrix. As they used time of flight (TOF) measurements for the determination of the charge carrier mobility of the molecularly doped polycarbonate, their data are not directly comparable to our results obtained from OTFT measurements which include device parameters and not only parameters of the material itself. In addition, we investigate bulk materials where direct contacts between our dipolar dyes are unavoidable. As depicted in **Figure 8**, the molecules investigated by Sugiuchi and Nishizawa show indeed the predicted relationship, i.e., a linear decrease of log μ with the square of the dipole moment of the organic semiconductor molecule.[15a] The most dipolar compounds might indicate a saturation behavior at charge carrier mobilities of ~10^{-7} cm^2 V^{-1} s^{-1} (for $\mu_g^2 < 25$ D^2) but due to the lack of more dipolar compounds in the given study this conclusion appears too speculative.

3.2. Impact of Molecule-Substrate and Dipolar Molecule-Molecule Interactions

This situation is now entirely different for our series of merocyanine dyes whose dipole moments cover a much larger range up to $\mu_g^2 > 200$ D^2. Our data show that the mobilities of the devices of the merocyanine dyes on the Si/SiO_2 substrate are not influenced by the dipole moment and vary in a non-ordered manner between 10^{-4}–10^{-6} cm^2 V^{-1} s^{-1} (filled squares

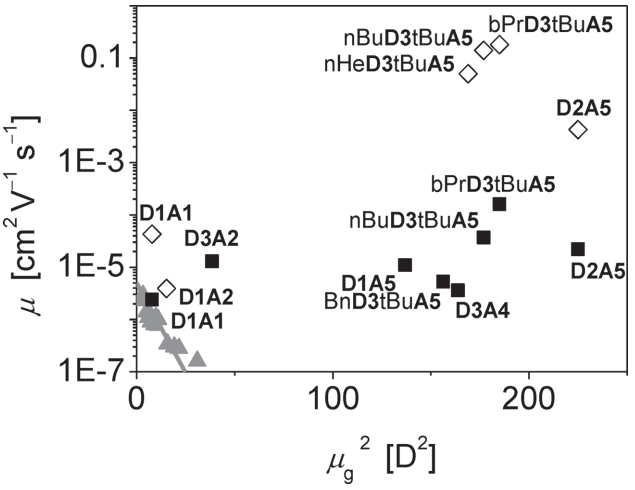

Figure 8. Dependance of the OTFT hole mobilities on the ground state dipole moments of the D–A dyes. The values are given for the thin films on the untreated Si/SiO_2 (filled squares) as well as on the TPA modified substrate (open squares). Additionally, the mobilities from Sugiuchi and Nishizawa[38] (grey triangles) with their linear fit from Dieckmann et al.[15a] (grey line) are shown.

in Figure 8). In order to rationalize these results with the previously described model, it must be addressed if the dipole moments in the thin films are non-interacting with respect to the thin film morphology. As merocyanine dyes are highly dipolar (μ_g up to 15.0 D, Table 1) and the films only consist of organic semiconductor molecules without any polymer matrix, the molecules will for sure interact. However, for the OTFT architecture, where charge transport takes place in the first layers of the interface, the interaction between substrate and semiconducting molecules has to be taken into account as well. As the mobilities of the OTFTs of our dyes on the Si/SiO_2 substrate show no clear dependance on the dipole moment (see Figure 8) and the AFM results indicate an amorphous morphology, the interaction between the molecules and the substrate probably superimposes the dipole-dipole interaction. Hence, the lack of influence on the packing from dipole-dipole interaction is ensured by the higher interaction between the substrate and the respective dye. The fact that the investigated merocyanines do not form ordered monolayers has recently also been confirmed for thin films on a Au(111) surface.[28]

Notably, although being a device parameter, the mobility of the OTFT with the least dipolar dye **D1A1** as organic semiconductor seems to loosely fit into the range of the mobility values which are predicted by Dieckmann, Bässler and Borsenberger. In contrast, looking at the mobility values for the more dipolar dyes on Si/SiO_2, these do not show a $\log \mu \sim -\mu_g^2$ behavior over the investigated range of dipole moments. This can be explained by the growing dipole-dipole interaction with higher dipolarity of the molecules as the electrostatic energy between two dipoles correlates quadratically with the dipole moment. Thus, the dipole-dipole interaction becomes more important regarding film formation although still not being the morphology determining factor. Still, as Dieckmann, Bässler and Borsenberger already mentioned in their study, deviations from the model for higher dipole moments ($\mu_g > 5$ D) clearly show the importance of dipole-dipole interactions which tend to align in an antiparallel manner in unpolar environment. Accordingly, our study corroborates that antiparallel aligned dimers are formed, which can be regarded as an unpolar moiety and will therefore not broaden the density of states as expected from a random orientation of dipole moments.

For the TPA modified surface, the case is different. As the surface energy is significantly reduced in comparison to the untreated Si/SiO_2,[39] it can be expected that there is a lower degree of interaction between organic molecules and the TPA functionalized surface than with the Si/SiO_2 surface. This has already been stated for thin films of pentacene on TPA as well as on other functionalized surfaces.[39,40] Consequently, the intermolecular forces now dominate the film formation which is supported by the AFM results showing clear structural features rather than unstructured amorphous surfaces of the thin films on the TPA modified substrate (Figure 4). Therefore, the relationship between charge carrier mobility and dipole moment will be completely different from the $\log \mu \sim -\mu_g^2$ behavior predicted for randomly disordered molecules. Our study shows that in the case of low dipole moments of ~3–6 D the reduced interaction between the surface and the molecule leads to a dewetting of the surface (Figure 4c,d) or to the formation of amorphous structures, which are not favorable for providing high charge carrier mobilities. Therefore for the dyes with low dipole moments, the corresponding mobilities fall into the same range as for the devices on Si/SiO_2. This corresponds well with the single crystal structures of these dyes which show only a low dimensional ordering of the molecules. On the other hand, for dyes bearing a larger dipole moment of 13–15 D, the high dipole-dipole interaction directs a highly ordered layer-like packing motif (Figure 5c,d) and the mobility even increases significantly by up to four orders of magnitude to yield a maximum of 0.18 $cm^2\ V^{-1}\ s^{-1}$ (open symbols in Figure 8).

3.3. Electrostatic Surface Potentials for Dye Monomers and Dimers

To elucidate why packing arrangements with different dimensional ordering (isolated dimers/tilted stacks in contrast to equidistant layers; Figure 5a,b vs Figure 5c,d) are formed for the given series of molecules, DFT calculations were performed to visualize the electrostatic potential on the van-der-Waals surface of appropriate dimers taken from the crystal structure. For comparison, the electrostatic potentials of the respective monomers were calculated as well and are shown together with those of the dimers in **Figure 9** (exemplarily shown are the electrostatic potentials of dyes **D3A1**, **D3A2** and nBu**D3**tBu**A5**; the results for dye Me**D3**tBu**A5** can be found in Supporting Information Figure S9). The monomers of all dyes clearly show the dipolar character of the molecules as well-defined centers of electron density can be seen. However, as expected based on our experimental data (Table 1), the dipolar nature of dye nBu**D3**tBu**A5** is also most pronounced in the calculation. Going from the monomer to the dimer, the electrostatic potential for dye **D3A1** becomes quite homogeneous throughout the molecular backbone, therefore illustrating the approach of the "supramolecular synthon". The centrosymmetric dimer can thus be regarded as

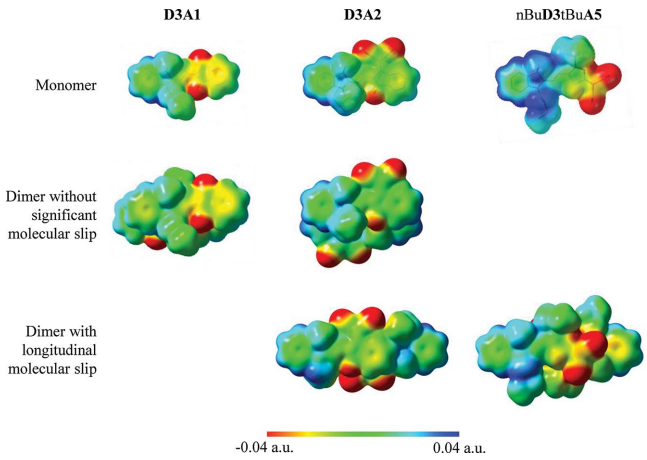

Figure 9. Electrostatic potential on the van-der-Waals surface of monomers and dimers of dyes **D3A1**, **D3A2** and nBu**D3**tBu**A5** (obtained for an isovalue of 0.001). The geometries of the monomers and dimers were taken from the crystal structures.

an unpolar moiety (see also Figure 5a). For dye nBu**D3**tBu**A5**, the dimer is again less polar than the monomer but a slight dipolar character for both molecules is still retained as the molecules are slipped against each other and mainly overlap with their acceptor parts (see also Figure 5d). This slip arises from the sterical demand of the bulky *tert*-butyl group attached to the acceptor and the $C(Me)_2$ group at the donor part. In this case, the polar surfaces are not fully covered and can induce an ordered alignment of other neighboring molecules. Dye **D3A2** seems to fall just in between these two cases as two non-equivalent dimers can be found in the crystal structure, one with a longitudinal molecular slip due to the $C(Me)_2$ group as well as the *n*-butyl chain and one without. The electrostatic potential of the dimer with a molecular slip again shows a slight dipolar character of both molecules whereas the result of the dimer with almost no molecular slip exhibits a more homogeneous electrostatic potential throughout the molecular backbone without fully annihilating the dipolar character. Still, this indicates a higher compensation of the molecular dipoles than for the dimer with the slipped arrangement and can be compared to the case of dye **D3A1**.

3.4. Rationalization of the Two Types of Packing

The two types of packing arrangements of our dyes (layers vs isolated dimers/tilted stacks) on the TPA modified substrate can be explained as follows: Due to the dipole-dipole interaction, which acts over a long range, all dyes assemble with next neighbors in an antiparallel fashion. For the dimers of dye **D3A1**, the molecules are well-stacked on top of each other (donor on top of acceptor), hence yielding a compensation of the electrostatic potential and cancelling out the dipole moments. However, dispersion interactions (e.g., van-der-Waals interactions), determined mainly by the sterics of the molecules' substituents, are relevant as well and can lead to slipped arrangements where the acceptor parts of neighboring molecules overlap with each other. Hence, for dye **D3A2** a dimer with this longitudinal slip can be found in the crystal structure. However, when such a dimer is formed, the next molecule—like for dye **D3A1**—can pack in such a way as to align antiparallel exactly on top of one molecule of the slipped dimer. If such a well-aligned dimer without or with only small molecular displacement is formed during the growth of a crystal, there is no further driving force to induce a highly ordered packing (especially for dyes with a low dipole moment) which ultimately results in isolated dimers (dye **D3A1**, Figure 5a) or tilted stacks of dimers (dye **D3A2**, Figure 5b).

The impact of sterics on the molecular packing can also be seen in the case of dye **D3A4**. Due to the high dipole moment of 12.8 D the tendency to pack in a layer-like motif can be clearly seen (Figure S7a). However, the sterical hindrance by the butyl chain at the acceptor and the two methyl groups at the donor part is too big. When a slipped dimer with overlapping acceptor parts is formed, the next molecule can only be located in such a way as to have a small overlap with the π-system of the dimer molecules. Therefore, only stacks which are twisted against each other can be formed. Presumably, if there was less sterical hindrance, the dyes would again form stacks of dimers with significant π-overlap which has already been shown for similar dyes in crystal structures as well as by the formation of dimer aggregates in solution for highly dipolar molecules even with no sterical hindrance.[20d,41] For the dyes of the **D3A5** family, dipolarity and sterics are balanced just right to direct the desired two-dimensional layer arrangement on the transistor dielectric. The two methyl groups at the donor part and the *tert*-butyl group at the acceptor moiety lead to a slip of the molecules (Figure 5c,d; Supporting Information Figure S7b,c), hence sustaining the dipolar character of the molecules in a centrosymmetric dimer unit. Therefore the large dipole moment can give rise to the growth of a 2D brickwork-type crystal structure.

Rephrasing, for merocyanines and presumably also for any D–A push-pull dye scaffold the dipole moment—together with well-designed sterics of the molecule—actually play the key role in the formation of well-ordered packing motifs as it induces highly ordered 2D layer-like crystal structures, which enable decent device performance. This is in contrast to former belief that molecules with high dipole moments should not be used for applications where a high charge carrier mobility is needed. In fact, our study even suggests that if molecules with dipole moments are used as semiconductors in OTFTs, the dipole moment has to be sufficiently high to induce an advantageous intimate packing of the dyes which will ultimately result in good charge carrier mobility values of the device. It might even be speculated that the strong Coulomb interaction between appropriately packed dipolar dyes might enable closer π–π- contacts below typical van-der-Waals distances and concomitantly larger transfer integrals (which depend by e^{-r} on distance).

4. Conclusion

We systematically investigated twenty merocyanine dyes composed of various donor and acceptor moieties with respect to their suitability as p-type semiconductors in organic thin film

transistors on two different substrates. Our studies show that the vast majority of the thin films formed by these dipolar D–A dyes are amorphous, even after tedious variation of substrate temperature and deposition rate. Thus, if at all, only low hole charge carrier mobilities around 10^{-4}–10^{-6} cm^2 V^{-1} s^{-1} were determined for these OTFTs on Si/SiO_2 in air. As an exception, among the most dipolar subseries (~13 D) containing 2-(4-alkylthiazol-2(3H)-ylidene)malononitrile acceptor and 1-alkyl-3,3-dimethylindolin-2-ylidene donor units, several dyes of the **D3A5** family could be identified that showed remarkably improved performance with mobilities of up to 0.18 cm^2 V^{-1} s^{-1} on substrates modified with a self-assembled monolayer of TPA. Comparison of the obtained mobility values to Bässler's disorder charge transport theory shows that our mobility values do not match the predicted log $\mu \sim -\mu_g^2$ behavior and show no significant scaling with the dipole moment on Si/SiO_2. This is explained by the formation of centrosymmetric dimers in the amorphous films which do not lower the mobility as expected. On the TPA modified substrate, the mobility values even increase with increasing dipole moments, indicating the formation of highly crystalline films for the **D3A5** family. Whereas all thin films of merocyanines are built up from antiparallel aligned dimers, the outstanding feature of these **D3A5** dyes is that they all crystallize in a two-dimensional layer-like structure with slipped π-stacking arrangements, which could be confirmed by SAED, XRD and single crystal structure analysis. From the calculated electrostatic surface potentials it seems rational that these two-dimensional brickwork-type patterns are formed due to the well-balanced sterics as well as the high dipolarity of the respective dyes. In this regard, properly positioned bulky substituents prohibit the dyes from forming isolated dimers with no overall dipole moment and yield a longitudinally slipped dimer unit in which the dipolar character of the molecules is retained. From our study it appears that it is not the molecules' dipolarity that limits the suitability of D–A molecules in organic electronics but the difficulty encountered for dipolar molecules to assemble in large crystalline domains on planar substrates. If this issue is solved, D–A dyes crystallizing with closer π–π-contacts might yield OTFTs with even higher charge carrier mobilities, approaching or even surpassing the currently best organic semiconductors.

5. Experimental Section

The synthesis of dyes **D3A1**,[28] **D3A2**,[20a] **D3A4**,[17b] nBu**D3**tBu**A5**,[28] nHe**D3**tBu**A5**,[42] Bn**D3**tBu**A5**,[20a] nBu**D3**nBu**A5**,[22] and bPr**D3**tBu**A5**[25] has been reported previously. The synthesis of all other dyes can be found in the Supporting Information.

Film and Transistor Fabrication: 30 nm thin merocyanine films were vacuum deposited either onto Si/SiO_2 substrates (100 nm dielectric layer; capacitance C_i = 34 nF cm^{-2}) as well as *n*-tetradecylphosphonic acid (TPA) modified Si/SiO_2 (100 nm)/AlO_x (8 nm) substrates (1.7 nm TPA monolayer; capacitance C_i = 32.4 nF cm^{-2}). During the deposition of the merocyanine dyes, a growth rate of 0.2–1.0 nm min^{-1} was adjusted by monitoring the film growth with a quartz crystal microbalance and the pressure was below 10^{-6} mbar. Furthermore, the substrate temperature (T_S) was kept constant at a fixed temperature in the range of 50–125 °C in order to obtain devices with optimized performance. Subsequently, 30 nm gold were evaporated through steel shadow masks onto the films to form the source and drain electrodes, finally yielding devices with a channel length *L* and width *W* of 100 and 200 µm, respectively.

Film Characterization: The transistor current voltage characteristics were measured under ambient conditions using a Micromanipulator 4060 and Agilent 4155C semiconductor parametric analyzer (Agilent Technologies, Inc., Santa Clara, CA), keeping the devices at 298 K. Prior to the characterization, the semiconducting film around the device was scratched with a needle of the used Micromanipulator to electrically isolate the device. Atomic force microscopy was carried out with a Bruker AXS MultiMode Nanoscope IV instrument in the tapping mode. Silicon cantilevers (OMCL-AC160TS, Olympus) with a spring constant of 42 N m^{-1} and a resonance frequency of ≈300 kHz were used. XRD experiments were performed on a Bruker D8 discovery thin film diffractometer with Cu K_α radiation (λ = 1.54056 Å) at a selected voltage of 40 kV and a current of 40 mA. The selected area electron diffraction was measured with a JEOL JEM-1011 transmission electron microscope at 100 kV. The fabrication of the SAED sample was according to ref.[43] and dark field was used for experiments to provide weaker-intensity beam and high contrast.

Crystal Structure Determination: The collection of crystallographic data of dyes **D3A1** and **D3A2** was done using a Bruker X8 APEX diffractometer while the data for dye **D3A4** was obtained with a Nonius KappaCCD instrument. Both diffractometers were equipped with a CCD area detector and used Mo K_α radiation (λ = 0.71073 Å). The crystallographic data of dyes Me**D3**tBu**A5**, nBu**D3**tBu**A5**, nHe**D3**tBu**A5** and bPr**D3**tBu**A5** was collected using a Bruker D8 Quest diffractometer with a Photon 100 CMOS APS detector and Cu K_α radiation (λ = 1.54056 Å). Solution of the structure was done with direct methods, refinement with the SHELX software package and expanding using Fourier techniques.[44] Non-hydrogen atoms were refined anisotropically while hydrogen atoms were positioned onto idealized positions and included in calculations of structure factors. CCDC 1017506–1017512 contains the supplementary crystallographic data for this paper. These data can be obtained free of charge from The Cambridge Crystallographic Data Center via www.ccdc.cam.ac.uk/data_request/cif.

DFT Calculations: DFT calculations were performed as single-point calculations with the Gaussian 09 software package[45] with the functional B3LYP[46] and the basis set 6–31G(d). The geometries of the monomers and dimers were taken from the crystal structure. The electrostatic surface potentials were then simulated from the data with the software package GaussView 5.[47]

Supporting Information

Supporting Information is available from the Wiley Online Library or from the author.

Acknowledgements

This work was financially supported by the German Federal Ministry of Science and Education (BMBF) within the LOTsE project. The authors thank Dr. Hannah Bürckstümmer, Dr. Elena Tulyakova, Manuela Kaiser and Christian Simon for the synthesis of some of the described dyes as well as Astrid Kudzus for processing of some compounds. The authors also thank Dr. Hagen Klauk and Dr. Ute Zschieschang (MPI für Festkörperforschung, Stuttgart) for providing TPA modified substrates and Dr. Christian Lehmann and Dr. Ebru Duman (MPI für Kohlenforschung, Mülheim) for the single crystal X-ray analysis of dye **D3A4**. Furthermore, the authors are grateful to Prof. Klaus Meerholz (Universität zu Köln) and his co-workers for many fruitful discussions on merocyanine based organic semiconductors during more than a decade of collaboration in the field of photorefractive and photovoltaic materials.

Received: August 7, 2014
Revised: September 11, 2014
Published online: October 13, 2014

[1] J. E. Anthony, *Angew. Chem.* **2008**, *120*, 460; *Angew. Chem. Int. Ed.* **2008**, *47*, 452.
[2] J. Mei, Y. Diao, A. L. Appleton, L. Fang, Z. Bao, *J. Am. Chem. Soc.* **2013**, *135*, 6724.
[3] C. Wang, H. Dong, W. Hu, Y. Liu, D. Zhu, *Chem. Rev.* **2012**, *112*, 2208.
[4] G. Schweicher, Y. Olivier, V. Lemaur, Y. H. Geerts, *Isr. J. Chem.* **2014**, *54*, 595.
[5] M. J. Kang, I. Doi, H. Mori, E. Miyazaki, K. Takimiya, M. Ikeda, H. Kuwabara, *Adv. Mater.* **2011**, *23*, 1222.
[6] A. Y. Amin, A. Khassanov, K. Reuter, T. Meyer-Friedrichsen, M. Halik, *J. Am. Chem. Soc.* **2012**, *134*, 16548.
[7] H. Minemawari, T. Yamada, H. Matsui, J. Tsutsumi, S. Haas, R. Chiba, R. Kumai, T. Hasegawa, *Nature* **2011**, *475*, 364.
[8] H. Usta, C. Newman, Z. Chen, A. Facchetti, *Adv. Mater.* **2012**, *24*, 3678.
[9] M. Zhang, H. N. Tsao, W. Pisula, C. Yang, A. K. Mishra, K. Müllen, *J. Am. Chem. Soc.* **2007**, *129*, 3472.
[10] H. N. Tsao, D. M. Cho, I. Park, M. R. Hansen, A. Mavrinskiy, D. Y. Yoon, R. Graf, W. Pisula, H. W. Spiess, K. Müllen, *J. Am. Chem. Soc.* **2011**, *133*, 2605.
[11] T. Lei, J.-H. Dou, J. Pei, *Adv. Mater.* **2012**, *24*, 6457.
[12] H.-R. Tseng, L. Ying, B. B. Y. Hsu, L. A. Perez, C. J. Takacs, G. C. Bazan, A. J. Heeger, *Nano Lett.* **2012**, *12*, 6353.
[13] H. Chen, Y. Guo, G. Yu, Y. Zhao, J. Zhang, D. Gao, H. Liu, Y. Liu, *Adv. Mater.* **2012**, *24*, 4618.
[14] J. Li, Y. Zhao, H. S. Tan, Y. Guo, C.-A. Di, G. Yu, Y. Liu, M. Lin, S. H. Lim, Y. Zhou, H. Su, B. S. Ong, *Sci. Rep.* **2012**, *2*, 754.
[15] a) A. Dieckmann, H. Bässler, P. M. Borsenberger, *J. Chem. Phys.* **1993**, *99*, 8136; b) D. Hertel, H. Bässler, *ChemPhysChem* **2008**, *9*, 666.
[16] a) L. Beverina, G. A. Pagani, *Acc. Chem. Res.* **2014**, *47*, 319; b) L. R. Dalton, P. A. Sullivan, D. H. Bale, *Chem. Rev.* **2010**, *110*, 25; c) A. Mishra, R. K. Behera, P. K. Behera, B. K. Mishra, G. B. Behera, *Chem. Rev.* **2000**, *100*, 1973; d) S. R. Marder, B. Kippelen, A. K.-Y. Jen, N. Peyghambarian, *Nature* **1997**, *388*, 845.
[17] a) F. Würthner, R. Wortmann, K. Meerholz, *ChemPhysChem* **2002**, *3*, 17; b) F. Würthner, R. Wortmann, R. Matschiner, K. Lukaszuk, K. Meerholz, Y. DeNardin, R. Bittner, C. Bräuchle, R. Sens, *Angew. Chem.* **1997**, *109*, 2933: *Angew. Chem. Int. Ed.* **1997**, *36*, 2765; c) S. Beckmann, K.-H. Etzbach, P. Krämer, K. Lukaszuk, R. Matschiner, A. J. Schmidt, P. Schuhmacher, R. Sens, G. Seybold, R. Wortmann, F. Würthner, *Adv. Mater.* **1999**, *11*, 536.
[18] a) A. K.-Y. Jen, Y. Liu, L. Zheng, S. Liu, K. J. Drost, Y. Zhang, L. R. Dalton, *Adv. Mater.* **1999**, *11*, 452; b) C. B. Gorman, S. R. Marder, *Proc. Natl. Acad. Sci. U.S.A.* **1993**, *90*, 11297; c) F. Terenziani, O. Mongin, C. Katan, B. K. G. Bhatthula, M. Blanchard-Desce, *Chem. Eur. J.* **2006**, *12*, 3089.
[19] a) A. Mishra, M. K. R. Fischer, P. Bäuerle, *Angew. Chem.* **2009**, *121*, 2510; *Angew. Chem. Int. Ed.* **2009**, *48*, 2474; b) A. Hagfeldt, G. Boschloo, L. Sun, L. Kloo, H. Pettersson, *Chem. Rev.* **2010**, *110*, 6595.
[20] a) N. M. Kronenberg, M. Deppisch, F. Würthner, H. W. A. Lademann, K. Deing, K. Meerholz, *Chem. Commun.* **2008**, 6489; b) H. Bürckstümmer, N. M. Kronenberg, M. Gsänger, M. Stolte, K. Meerholz, F. Würthner, *J. Mater. Chem.* **2010**, *20*, 240; c) N. M. Kronenberg, V. Steinmann, H. Bürckstümmer, J. Hwang, D. Hertel, F. Würthner, K. Meerholz, *Adv. Mater.* **2010**, *22*, 4193; d) H. Bürckstümmer, E. V. Tulyakova, M. Deppisch, M. R. Lenze, N. M. Kronenberg, M. Gsänger, M. Stolte, K. Meerholz, F. Würthner, *Angew. Chem.* **2011**, *123*, 11832; *Angew. Chem. Int. Ed.* **2011**, *50*, 11628.
[21] a) Y.-H. Chen, L.-Y. Lin, C.-W. Lu, F. Lin, Z.-Y. Huang, H.-W. Lin, P.-H. Wang, Y.-H. Liu, K.-T. Wong, J. Wen, D. J. Miller, S. B. Darling, *J. Am. Chem. Soc.* **2012**, *134*, 13616; b) S.-W. Chiu, L.-Y. Lin, H.-W. Lin, Y.-H. Chen, Z.-Y. Huang, Y.-T. Lin, F. Lin, Y.-H. Liu, K.-T. Wong, *Chem. Commun.* **2012**, *48*, 1857.
[22] A. Ojala, H. Bürckstümmer, J. Hwang, K. Graf, B. von Vacano, K. Meerholz, P. Erk, F. Würthner, *J. Mater. Chem.* **2012**, *22*, 4473.
[23] A. Ojala, A. Petersen, A. Fuchs, R. Lovrincic, C. Pölking, J. Trollmann, J. Hwang, C. Lennartz, H. Reichelt, H. W. Höffken, A. Pucci, P. Erk, T. Kirchartz, F. Würthner, *Adv. Funct. Mater.* **2012**, *22*, 86.
[24] K. Kudo, M. Yamashina, T. Moriizumi, *Jpn. J. Appl. Phys.* **1984**, *23*, 130.
[25] L. Huang, M. Stolte, H. Bürckstümmer, F. Würthner, *Adv. Mater.* **2012**, *24*, 5750.
[26] E. Fischer, A. Steche, *Liebigs Ann. Chem.* **1887**, *242*, 348.
[27] F. Würthner, *Synthesis* **1999**, *12*, 2103.
[28] S. Krause, M. Stolte, F. Würthner, N. Koch, *J. Phys. Chem. C* **2013**, *117*, 19031.
[29] F. Würthner, S. Yao, R. Wortmann, *Polym. Mater. Sci. Eng.* **2000**, *83*, 186.
[30] L. Onsager, *J. Am. Chem. Soc.* **1936**, *58*, 1486.
[31] a) N. G. Connelly, W. E. Geiger, *Chem. Rev.* **1996**, *96*, 877; b) W. N. Hansen, G. J. Hansen, *Phys. Rev. A* **1987**, *36*, 1396; c) C. M. Cardona, W. Li, A. E. Kaifer, D. Stockdale, G. C. Bazan, *Adv. Mater.* **2011**, *23*, 2367.
[32] R. P. Shibaeva, E. B. Yagubskii, *Chem. Rev.* **2004**, *104*, 5347.
[33] J. J. Wolff, R. Wortmann, in *Advances in Physical Organic Chemistry* Vol. *32* (Ed: D. Bethell), Academic Press, New York, USA **1999**, Ch. 2.
[34] For the related parameters MIX and BLA that are accessed by other experimental techniques, see: a) S. R. Marder, C. B. Gorman, F. Meyers, J. W. Perry, G. Bourhill, J.-L. Brédas, B. M. Pierce, *Science* **1994**, *265*, 632; b) M. Barzoukas, C. Runser, A. Fort, M. Blanchard-Desce, *Chem. Phys. Lett.* **1996**, *257*, 531.
[35] F. Würthner, K. Meerholz, *Chem. Eur. J.* **2010**, *16*, 9366.
[36] G. R. Desiraju, *Angew. Chem.* **1995**, *107*, 2541; *Angew. Chem. Int. Ed. Engl.* **1995**, *34*, 2311.
[37] C. F. Macrae, P. R. Edgington, P. McCabe, E. Pidcock, G. P. Shields, R. Taylor, M. Towler, J. van de Streek, *J. Appl. Cryst.* **2006**, *39*, 453.
[38] M. Sugiuchi, H. Nishizawa, *J. Imag. Sci. Technol.* **1993**, *37*, 245.
[39] S. Yogev, R. Matsubara, M. Nakamura, U. Zschieschang, H. Klauk, Y. Rosenwaks, *Phys. Rev. Lett.* **2013**, *110*, 036803.
[40] A. Amassian, V. A. Pozdin, T. V. Desai, S. Hong, A. R. Woll, J. D. Ferguson, J. D. Brock, G. G. Malliaras, J. R. Engstrom, *J. Mater. Chem.* **2009**, *19*, 5580.
[41] F. Würthner, S. Yao, T. Debaerdemaeker, R. Wortmann, *J. Am. Chem. Soc.* **2002**, *124*, 9431.
[42] A. Ojala, H. Bürckstümmer, M. Stolte, R. Sens, H. Reichelt, P. Erk, J. Hwang, D. Hertel, K. Meerholz, F. Würthner, *Adv. Mater.* **2011**, *23*, 5398.
[43] L. Huang, F. Zhu, C. Liu, H. Wang, Y. Geng, D. Yan, *Org. Electron.* **2010**, *11*, 195.
[44] G. M. Sheldrick, *Acta Crystallogr., Sect. A: Found. Crystallogr.* **2008**, *A64*, 112.
[45] Gaussian 09, Revision D.01, M. J. Frisch, G. W. Trucks, H. B. Schlegel, G. E. Scuseria, M. A. Robb, J. R. Cheeseman, G. Scalmani, V. Barone, B. Mennucci, G. A. Petersson, H. Nakatsuji, M. Caricato, X. Li, H. P. Hratchian, A. F. Izmaylov, J. Bloino, G. Zheng, J. L. Sonnenberg, M. Hada, M. Ehara, K. Toyota, R. Fukuda, J. Hasegawa, M. Ishida, T. Nakajima, Y. Honda, O. Kitao, H. Nakai, T. Vreven, J. A. Montgomery Jr., J. E. Peralta, F. Ogliaro, M. Bearpark, J. J. Heyd, E. Brothers, K. N. Kudin, V. N. Staroverov, R. Kobayashi, J. Normand, K. Raghavachari, A. Rendell, J. C. Burant, S. S. Iyengar, J. Tomasi, M. Cossi, N. Rega, J. M. Millam, M. Klene, J. E. Knox, J. B. Cross, V. Bakken, C. Adamo, J. Jaramillo, R. Gomperts, R. E. Stratmann, O. Yazyev, A. J. Austin, R. Cammi, C. Pomelli, J. W. Ochterski, R. L. Martin, K. Morokuma, V. G. Zakrzewski, G. A. Voth, P. Salvador, J. J. Dannenberg, S. Dapprich, A. D. Daniels, Ö. Farkas, J. B. Foresman, J. V. Ortiz, J. Cioslowski, D. J. Fox, Gaussian, Inc., Wallingford CT, 2009.
[46] a) A. D. Becke, *Phys. Rev. A* **1988**, *38*, 3098; b) C. Lee, W. Yang, R. G. Parr, *Phys. Rev. B* **1988**, *37*, 785; c) A. D. Becke, *J. Chem. Phys.* **1993**, *98*, 5648.
[47] GaussView, Version 5, R. Dennington, T. Keith, J. Millam, Semichem Inc., Shawnee Mission KS, 2009.